Journal of Sound and Vibration 584 (2024) 118426

Contents lists available at ScienceDirect

Journal of Sound and Vibration

journal homepage: www.elsevier.com/locate/jsvi

Localised wavenumber estimation and its application to waveguide discontinuities

M.W. Bavaresco [a,*], E. Rustighi [b], N.S. Ferguson [a]

[a] Institute of Sound and Vibration Research, University of Southampton, Southampton, SO17 1BJ, UK
[b] Department of Industrial Engineering, University of Trento, Trento, Trentino-Alto Adige 38121-38123, Italy

ARTICLE INFO

Keywords:
Local wavenumber
Wavenumber estimation
Discontinuity
Localisation
Hilbert transform
Direct quadrature

ABSTRACT

Wave propagation methods have been widely investigated for the potential application to the detection and localisation of discontinuities in structural waveguides. In the low-mid frequency ranges, previous preliminary works that used the analytic signal theory have considered local wavenumber estimations based on the time domain for the purpose of localisation in mechanical structures. However, these have not fully exploited the potential of this approach. This is accomplished herein for a one-dimensional infinite-like waveguide by means of two methods applied in the spatial domain; namely the Hilbert transform via the wavenumber domain estimator and the Direct Quadrature method. Modifications are proposed to make these methods more suitable to the space-wavenumber application and for the purpose of localisation. A three-dimensional plot is proposed, where local divergences of the wavenumbers indicate the positions of the discontinuities for otherwise uniform waveguides. Numerical simulations and experiments show an accurate estimation of the local wavenumbers and validate the methods with the proposed modifications for the localisation of different types of discontinuities.

1. Introduction

Detection of discontinuities or local changes within structures is an important activity for health assessment and characterisation of structural components. The estimation of wavenumbers for structures can give information about discontinuities present in waveguides. Thus wavenumber estimation is a relevant topic in applications that require the understanding of wave propagation characteristics of structures including periodic features, damaged structures, complex geometries and others [1–4].

Wavenumbers have traditionally been evaluated through a global approach, where multiple measurement points along the structure are used to derive one space-invariant estimate [5–9]. A conventional spatial Fourier transform follows the same principle, as the signal under analysis is assumed to have space-invariant amplitude and wavenumbers. On the other hand, local approaches allow for the understanding of the wavenumber spatial distribution and its variation provides insight into the underlying properties or behaviour of the structure and potential structural changes.

A way to determine wavenumbers locally is through the windowed Fourier transform, where the Fourier transform is applied sequentially to consecutive sections of a structure, identifying local aspects in the spatial dimension. Methodologies based on this principle have been proposed to determine local wavenumbers with the purpose of locating discontinuities in a structure in the form of delamination in multi-layer composites [2,10-12], corrosion [13,14] and surface defects [15]. Although local quantities are identified,

* Corresponding author.
E-mail address: mwb1f19@soton.ac.uk (M.W. Bavaresco).

https://doi.org/10.1016/j.jsv.2024.118426
Received 12 November 2023; Received in revised form 2 March 2024; Accepted 3 April 2024
Available online 24 April 2024

these methodologies are based on a global approach approximated to a local one by spatial windowing. In this case, the wavenumber resolution is limited by the length of the spatial window.

Truly local quantities can be derived using the analytic signal theory, where local properties can be theoretically extracted for each measurement point instead of being approximated through a short-windowed version of the signal. The analytic signal is a complex-valued signal that contains information about the local amplitudes and local wavenumbers of a signal, thus allowing for their estimation. The determination of the analytic signal from a real-valued signal can be challenging, and there exist multiple methods to achieve this with the Hilbert transform being commonly used (Feldman [16]).

Note that this work specifically focuses on the local aspect of the wavenumbers. However, depending on the application, the time dependency is also important, for which the instantaneous aspect of wavenumbers can be explored. In both cases, the starting signals are waves measured in the spatial domain which are then analysed spatially to yield local wavenumbers or over time to yield instantaneous wavenumbers. Similarly, when the starting signals are oscillations in the time domain, local or instantaneous frequencies can be determined by considering either space or time appropriately in the derivation of the analytic signal.

The use of the Hilbert transform for the analytic signal calculation is commonly performed in the time-frequency domain, though it will be considered in this work for the space-wavenumber domain. The Hilbert transform is seen as an appropriate method to deal with non-linear and non-stationary problems, unlike the conventional Fourier spectral analysis [17], and is thus suitable for the localisation of a discontinuity in an otherwise uniform and homogeneous waveguide. A limitation of the Hilbert transform is that it is not directly applicable to broadband signals, i.e. multiple frequency components cannot exist simultaneously in the signal under analysis. In order to deal with broadband signals, Huang et al. [17–19] presented a method that is nowadays referred to as Hilbert-Huang transform which allowed for the estimation of multiple instantaneous frequencies based on the empirical mode decomposition. In the topic of anomalies detection, Quek, et al. [20] used Hilbert-Huang transformed signals to track the wave propagation times, which can give an indication of damage when additional wave reflections are observed in the data or due to differences in the propagation times (depending on the sensor setup). Bandara, et al. [21] also tracked changes in the instantaneous frequencies extracted through the Hilbert-Huang method and were thus able to detect damages in timber poles. Note that these previous works were limited to time-domain signals, i.e. the tracking of instantaneous frequencies. Mesnil, et al. [4] use both instantaneous and local wavenumber approaches for damage quantification in composite structures. The instantaneous wavenumber was derived through a Hilbert transform, but the local wavenumber was based on a windowed Fourier transform. The same approach was also investigated by Lugovtsova, et al. [22] for an aluminium carbon-fibre reinforced composite structure. Therefore, the Huang-Hilbert transform was limited to the instantaneous wavenumber estimation and not applied for the local wavenumber estimation. Craciunescu and Christou [23] recently cosidered the application of the Hilbert transform to characterise unsteady water waves in both time and spatial domains, being the space domain and local wavenumbers particularly of interest for this work. By comparison with other methods, they found low accuracy in the estimated wavenumbers through the Hilbert transform with results being 12 % underestimated whereas the Double Fourier method yielded only a 2 % error. However, as pointed out by the authors, no decomposition method was applied in the multi-component signal prior to the use of the Hilbert transform (as proposed by Huang et al. [17]). Overall, the Hilbert transform has not been properly used for the local wavenumber estimation and the tracking of changes in these quantities for discontinuity detection in waveguides. This is likely caused by the effects of truncation and Gibbs phenomenon in the frequency domain Hilbert estimator that bring distortions to the extracted wavenumbers (Feldman [16]). In this work, modifications are proposed in the data processing to avoid these distortions and render the Hilbert transform applicable to local wavenumber estimations.

An alternative method which does not rely on the Hilbert transform is also explored for the same purpose in this work, namely the Direct Quadrature. The Direct Quadrature method has been proposed to analyse time domain signals by Huang, et al. [24]. This is one of several alternative methods to calculate the instantaneous frequency of a signal without the need to calculate the analytic signal. A comparison with the Hilbert transform shows improvements brought about by the Direct Quadrature method, which will be explored in this work; albeit, the derivation here will be conducted in the spatial domain for the wavenumber estimation instead of the time domain.

This work's main contribution is that by using local wavenumber estimations, derived through either the Hilbert transform or the Direct Quadrature method, one can identify changes and locate a discontinuity or anomaly in a waveguide.

The issues arising from broadband signals are not investigated here, as only flexural waves of one-dimensional waveguides in the frequency domain are considered. That is, a single wavenumber is assumed to exist locally at each frequency. Each frequency is considered separately, thus eliminating the need to apply any method to deal with synchronous multiple components. However, if the methods presented here are to be employed on signals with multiple synchronous components, a prior reduction of the signal such as the empirical mode decomposition should be performed (Huang, et al. [17]). Another challenge to be considered in applying these methods to other wave types is related to the realisation of the experiment, as some wave types, e.g. longitudinal, might be difficult to excite and measure.

The next section contains an overview of the relevant methods, including the definition of the local wavenumber as a property of the analytic signal, and the descriptions of the Hilbert transform and the Direct Quadrature, along with the main sources of distortions and the proposed modifications to make these methods more suitable to the application at hand. A numerical analysis is then performed where an infinite one-dimensional waveguide is simulated, and the two methods are employed to locate a structural change added to the structure. This is then validated experimentally with a beam with anechoic terminations and added discontinuities in the form of a mass or supporting string.

2. Methods

The methods reviewed and modified in this work are based on the local wavenumber defined as a property of the analytic signal. An analytic signal $z(x)$ is a complex-valued signal that has an imaginary part $\widetilde{w}(x)$ which corresponds to the quadrature of its real part $w(x)$ (Gabor [25]):

$$z(x) = w(x) + i\widetilde{w}(x) \tag{1}$$

Although commonly applied to time signals (Mesnil, et al. [4]), in this work the following theory is adapted to vibration signals over space. The real and imaginary components can be written as a function of their local amplitudes $A(x)$ and local arguments $\varphi(x)$

$$w(x) = A(x)\cos\varphi(x) \tag{2}$$

$$\widetilde{w}(x) = A(x)\sin\varphi(x) \tag{3}$$

Over a spatial length Δx, an average wavenumber is defined as

$$\overline{k} = \frac{\Delta\varphi}{\Delta x} \tag{4}$$

The local equivalent quantity is defined as the derivative of the angular value,

$$k(x) = \frac{\mathrm{d}\varphi(x)}{\mathrm{d}x} \tag{5}$$

Eq. (5) defines the local wavenumber $k(x)$ which can be determined for each point in space to evidence local characteristics of the signal, which in turn represent the waveguide. The difficulty thus lies in estimating the local wavenumber from the values of $w(x)$ as the starting point. Two methods are evaluated for this purpose, the Hilbert transform frequency domain estimator and the Direct Quadrature. Modifications are proposed to deal with the main distortions encountered with the methods and a general step-by-step is provided to facilitate the implementation of the algorithms of both methods.

As presented in the frequency-domain instantaneous wavenumber technique by Mesnil, et al. [4], the measurement data is first brought into the frequency domain so that at each frequency there is only one dominant flexural wavenumber in the data. Here, frequency response functions are used, which are complex-valued. Its real and imaginary parts are separated, and each is sequentially considered as the signal $w(x)$. Thus, two values of local wavenumbers are calculated, one from the real and one from the imaginary part of the FRF, and a final estimation is reached through averaging these results. This approach was taken to account for all information contained in the FRF as its real and imaginary parts might present different levels of contribution throughout the spectrum.

2.1. Analytic signal estimation through the pre-truncated hilbert transform

The Hilbert transform can be seen as an approach to calculate the quadrature of a real signal in order to form the analytic signal necessary for the extraction of local wavenumbers. As a convolution integral, the Hilbert transform is defined for a real-valued function $w(x)$ extending over a range $-\infty < x < \infty$ as the real-valued function $\widetilde{w}(x)$ (Bendat and Piersol [26]):

$$\widetilde{w}(x) = \mathscr{H}[w(x)] = \int_{-\infty}^{\infty} \frac{w(u)}{\pi(x-u)}\mathrm{d}u \tag{6}$$

Therefore $\widetilde{w}(x)$ is the convolution integral of $w(x)$ and $(1/\pi x)$, mathematically

$$\widetilde{w}(x) = w(x) * (1/\pi x) \tag{7}$$

Where * indicates the convolution operator. Now consider $\widetilde{W}(k)$ as the Fourier transform of $\widetilde{w}(x)$,

$$\widetilde{W}(k) = \mathscr{F}[\widetilde{w}(x)] = \int_{-\infty}^{\infty} \widetilde{w}(x)\mathrm{e}^{-\mathrm{j}kx}\mathrm{d}x \tag{8}$$

Using Eq. (7) and Eq. (8), $\widetilde{W}(k)$ can be seen as the Fourier transform of $w(x)$ multiplied by the Fourier transform of $(1/\pi x)$. This second term is given by

$$\mathscr{F}[1/\pi x] = -j\ \mathrm{sgn}\ k = \begin{cases} -j\ for\ k > 0 \\ 0\ for\ k = 0 \\ j\ for\ k < 0 \end{cases} \tag{9}$$

and the function sgn $k = 0$ at $k = 0$. In that way, the quantities $\widetilde{W}(k)$ and $W(k)$ can be related through

$$\widetilde{W}(k) = (-j\ \mathrm{sgn}\ k)W(k) \tag{10}$$

Note that $\widetilde{W}(k)$ is not the Hilbert transform of the complex-valued quantity $W(k)$. It is the Fourier transform of $\widetilde{w}(x)$, which in turn is

the Hilbert transform of $w(x)$.

A Hilbert transformer, which is an ideal phase shifter, cannot be realized digitally. Any practical filter would incur some loss characteristics, for which reason estimators are used as approximations for the Hilbert transform [16].

The estimator in the wavenumber domain is defined based on the relationships that exist between the Fourier transform of the real-valued signal, $W(k)$, and that of its quadrature $\widetilde{W}(k)$. These relationships evidence some characteristics about the Fourier transform of the analytic signal defined in Eq. (2.1). These are illustrated in Fig. 1.

In Fig. 1a, the plot illustrates the magnitude of the Fourier transform of a real-valued signal $w(x)$, whereas on Fig. 1b the magnitude of the Fourier transform of its analytic signal $z(x) = w(x) + j\widetilde{w}(x)$ is shown. The spectrum $Z(k)$ is shown to diverge from the spectrum $W(k)$ in two aspects: the spectrum $Z(k)$ obtained from the analytic signal does not contain a "mirrored effect" on the negative wavenumbers as it happens for $W(k)$ and the magnitude $|Z(k)|$ at the positive wavenumber components is twice that of the positive wavenumber components found in the magnitude $|W(k)|$. Through these relationships, the quantity $Z(k)$ can be found by extracting the one-sided spectrum of the quantity $W(k)$.

Starting from the real-valued function $w(x)$, its analytic signal $z(x)$ can be calculated by applying the Fourier transform to find $W(k)$, calculating its one-sided spectrum $Z(k)$ and performing an inverse Fourier transform to yield $z(x)$. This is referred to as the Hilbert transform estimator in wavenumber domain. Eq. (11) brings the real-valued signal $w(x)$ to the wavenumber domain through a discrete Fourier Transform (DFT), eliminates the negative wavenumber components and duplicates the magnitude of the positive wavenumber components,

$$z(x) = \mathscr{F}^{-1}\{C(n).\mathscr{F}[w(x)]\} \tag{11}$$

where $C(n) = 2$ for $n = \left\{0, \frac{N}{2} - 1\right\}$; $C(n) = 0$ for $n = \left\{\frac{N}{2}, N - 1\right\}$. Because it relies upon the discrete Fourier transform of the original signal, this method has the same truncation issues encountered with the DFT technique. In addition, it also suffers from Gibbs phenomenon, also known as an end effect (Feldman [16]).

2.1.1. Signal truncation to deal with gibbs phenomenon

Given the nature of the problem being tackled, Gibbs phenomenon is anticipated to affect the estimation of wavenumbers in two ways. First, because the measurements consist of truncated spatial arrays, Gibbs phenomenon will in the most cases distort the data as it is likely for the truncated signal to have discontinuities at their start and end measurements. Note that if the truncated signal would start and end in such a way to form complete periods, Gibbs phenomenon would be non-existent or extremely reduced depending on the discontinuities within the signal (Cheh [27]). Hence, the extremes of the data are likely to have distortions because of Gibbs phenomenon and those are carried into the spatial array as well. Secondly, the local structural changes may also cause distortions because of possible amplitude steps in the analytic signal, again related to Gibbs phenomenon (Feldman [16]). This second effect could even be beneficial for the localisation as it could magnify the structural change effect in the local wavenumber estimation rendering it more visible in the dispersion plot. Since the former effect could outweigh the distortions brought about by structural changes and make them invisible in the local wavenumber plot, a modification is proposed to avert it.

To deal with the first effect, the data is truncated prior to the application of the Hilbert transform at positions that ensure the signal extrema to be zero-valued. Only the rectangular type of window is considered, since the use of different types of windows would change the waveform of the signal, thus distorting local wavenumbers at the edges of the measurement array.

Fig. 2 is used to exemplify the truncation method. Fig. 2a presents the signal from which the local wavenumbers are to be extracted. If the Hilbert transform estimator is applied directly on this signal, the analytic signal is calculated through Eq. (11) and the resulting local wavenumbers through the numerical derivative of Eq. (5), resulting in the plot in Fig. 2b. This plot presents the estimated local wavenumbers as a function of space, $k(x)$, in red, along with the expected value, in the black dashed line. Gibbs phenomenon affects these results causing the estimated wavenumbers to oscillate around the true value along the data, with a greater impact at the initial and end points of the signal.

Alternatively, by first truncating the signal to the one shown in Fig. 2c and then using Eq. (5) and (11) to determine the local wavenumbers results in the plot shown in Fig. 2d. Note that the original signal is truncated into two signals (shown in the two shades of orange of Fig. 2c). For the truncation to take place, a cubic spline function is fitted using the MATLAB function `csapi` [28], and the

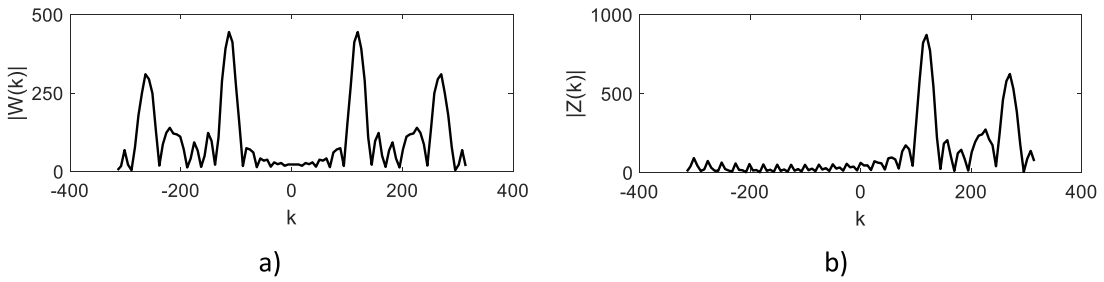

Fig. 1. Magnitude of the spectra of Fourier transform of the original signal or real part of an analytic signal (a) and the analytic signal (b) in the wavenumber domain.

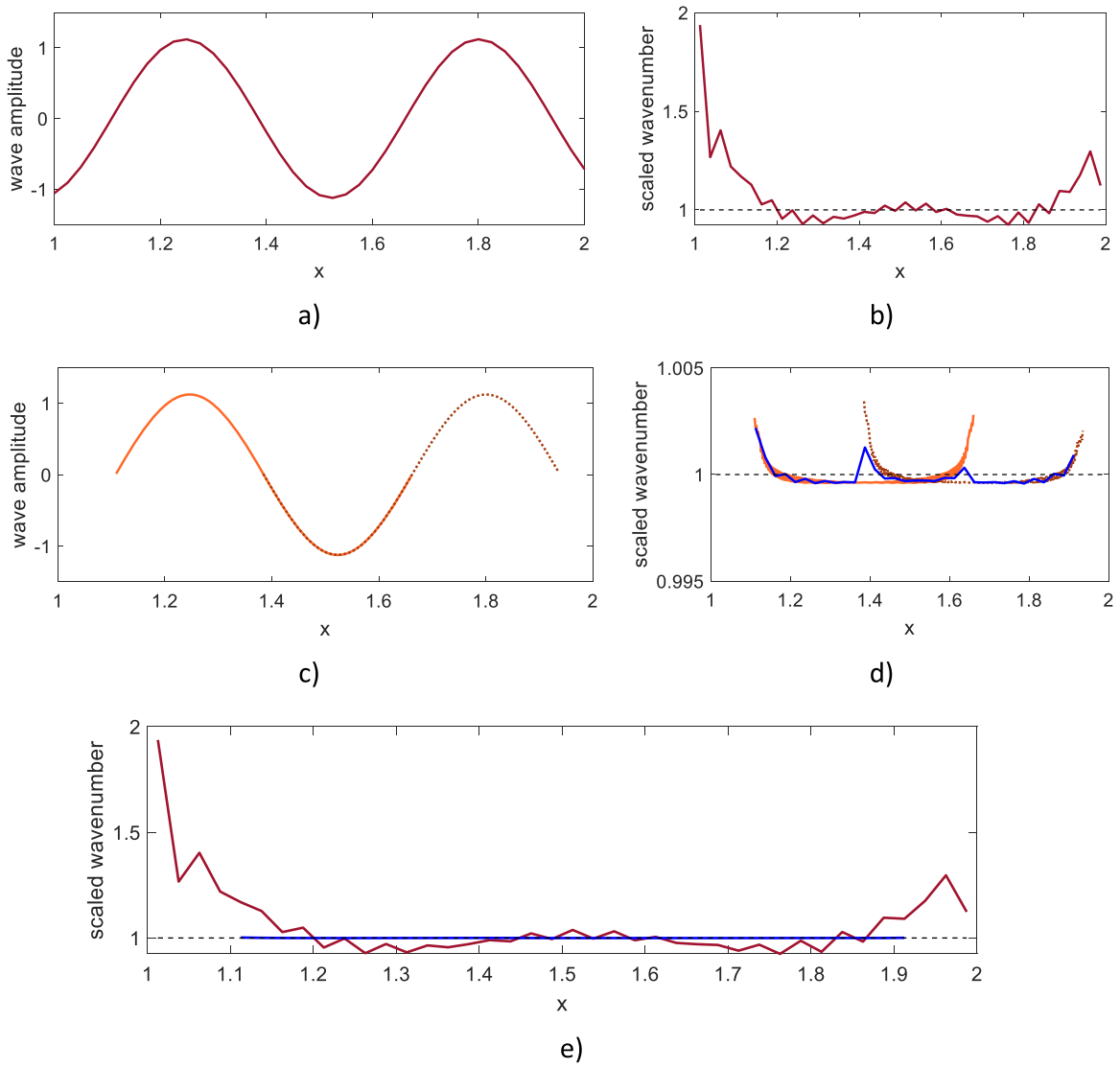

Fig. 2. Original signal (a) and calculated local wavenumbers through HT without pre-truncation (b): estimated wavenumber (continuous red line) and reference wavenumber (dashed black line). Pre-truncated wave signals (c) and local wavenumbers through HT with pre-truncation (d): estimated wavenumbers (continuous and dotted orange lines), averaged wavenumbers (continuous blue line) and reference value (dashed black line). Comparison (e) between estimated wavenumbers with (continuous blue line) and without pre-truncation (continuous red line) versus reference value (dashed black line). The estimated wavenumbers are scaled to the actual wavenumber.

number of data points is artificially increased to ensure the truncation can occur as close to the zero-crossing positions as possible. Note that the two sub-signals are generated in this example as the data contains 1.5 full wavelengths, meaning that starting from the left edge of the data, a full wavelength can be extracted that has an overlapping length with the full wavelength extracted starting from the right edge of the data. After the truncation, each sub-signal is processed through the Hilbert transform and the local wavenumbers calculated. Before returning to the original number of sampling points, a moving mean is applied to the local wavenumbers with a window that has the same size as the previously added sampling points. The result of this moving mean is shown in the orange curves of Fig. 2d. The results are then sampled back to the original sampling and because there is a range of two overlapping estimations, a mean is obtained between them, resulting in the blue curve shown in the same plot.

A comparison to the true wavenumber value and to the previous estimation demonstrates how the end effect is reduced in this case, see Fig. 2e. The drawback is the loss of data at the edges of the signal. However, given the extent to which the wavenumbers are affected by Gibbs phenomenon, it is preferable to lose information at the edges of the measurement array and be able to detect local structural change within the remaining array length rather than not being able to detect local changes given the distortions existing throughout the data.

2.1.2. Algorithm for the pre-truncated hilbert transform

This method will be referred to as the pre-truncated Hilbert transform in the following sections. As frequency response functions are used in this work as inputs to this method, their real and imaginary parts are analysed separately and at each frequency the steps summarized in Table 1 are taken.

Following the steps of Table 1, a weighted mean is calculated from the wavenumbers resulting from the real and imaginary parts of the frequency response functions. It is based on the rms values of the original signal at each frequency to ensure that the proper weight is given to structural results in comparison to the effects of noise.

Later, numerical and experimental studies are carried out to validate the use of local wavenumbers estimated through this method to locate a structural change added to a uniform and homogeneous waveguide. An alternative approach to this method is also explored in this work and is described in the next section.

2.2. Modified direct quadrature for local wavenumber estimation

This method was presented by Huang, et al. [24] as an alternative to the Hilbert transform in calculating the instantaneous frequency from a real-valued signal. It consists of applying an Amplitude and Frequency Modulated (AM-FM) decomposition to the signal, and from the FM part – or frequency carrier signal – determining the angular value $\varphi(x)$.

The AM-FM decomposition is a normalisation scheme which separates the amplitude and frequency information of the given signal in a unique and empirical way. As it happens for the application of the Hilbert transform, the signal $w(x)$ needs to be in the form of an Intrinsic Mode Function (IMF) before applying this technique. That is, the number of extrema and the number of zero-crossings along the entire signal must be equal or differ at most by one and the mean of the envelopes of the signal defined by the local maxima and local minima at any point is zero (Quek, et al. [20]). The following is a short review of the AM-FM decomposition as described in Huang, et al. [24]:

1. The envelope $e_1(x)$ of the IMF is calculated by locating all the local extrema from the absolute value of the reference signal and connecting those points with a cubic spline curve. If this is the first iteration, the reference signal is $W(x)$.
2. The reference signal is divided by the envelope $e_1(x)$ calculated in step 1 and the resulting value is defined as $w_2(x)$.
3. The resulting function $w_2(x)$ is evaluated. If $w_2(x)$ is scaled to unity, then $w_2(x)$ is considered the frequency carrier signal $F(x)$. If $w_2(x)$ is not properly normalised, then steps 1–2 are repeated until the resulting signal $w_n(x)$ is scaled to unity so that $F(x) = w_n(x)$.
4. The AM signal $A(x)$ can be calculated by dividing the original data $w(x)$ by the FM signal $F(x)$. In this work, the AM signal is not calculated as the interest lies on tracking the angular value $\varphi(x)$ of the signal only, and not its amplitude.

Fig. 3 exemplifies the single step AM-FM decomposition of a signal $w(x)$.

After obtaining the FM signal, $F(x)$, because it is an oscillation scaled to unity with a single wavenumber at each point, it can be assumed to be a cosine function, i.e.

$$F(x) = \cos\varphi(x) \tag{12}$$

whose Direct Quadrature is a sine of the same angular value $\varphi(x)$:

$$\sin\varphi(x) = \sqrt{1 - F(x)^2} \tag{13}$$

The angular value, which is needed for the calculation of the local wavenumber $k(x)$ as in Eq. (5), can be found through

$$\varphi(x) = \tan^{-1}\left(\frac{\sqrt{1 - F(x)^2}}{F(x)}\right) \tag{14}$$

Or simply through the relation

$$\varphi(x) = \cos^{-1}(F(x)\ ) \tag{15}$$

Note that through this method, the angular value $\varphi(x)$ is calculated without forming the analytic signal composed by the original

Table 1
Steps of the pre-truncated Hilbert transform method.

Steps	Purpose
Increase number of sampling points through cubic spline fitting	Addition of data points to ensure subsequent truncation occurs as close as possible to a zero-crossing
Truncate signal at zero-crossings to form full period(s)	To avoid distortions brought by Gibbs phenomenon
Apply Hilbert transform estimator	To obtain the analytic signal and extract local wavenumbers
Decrease number of sampling points	To return data points to the original measured positions
Average local wavenumber results if step 2 yields two overlapping signals	To have a single local wavenumber estimation

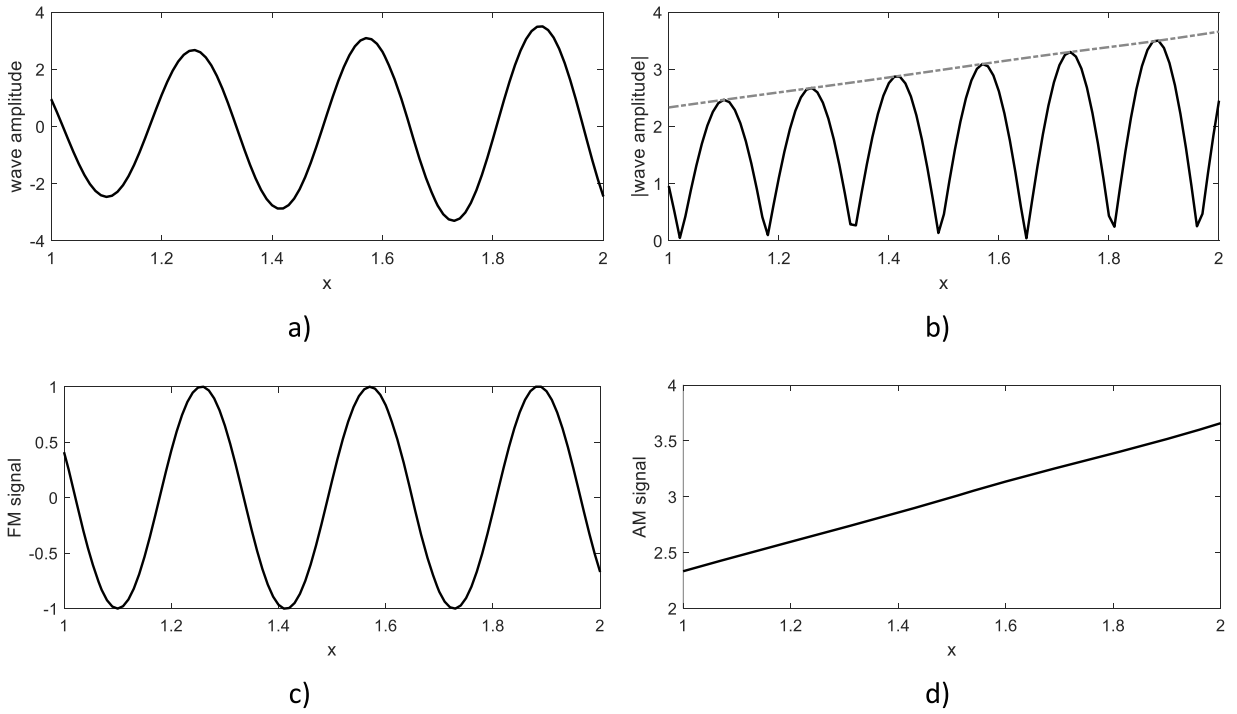

Fig. 3. Illustration of AM-FM decomposition: (a) signal prior to decomposition $W(x)$, (b) absolute value of signal $w(x)|$ (continuous black line) and envelope $e_1(x)$ (dash-dot grey line), decomposed (c) FM signal $F(x)$ and (d) AM signal.

signal and its quadrature. Instead, the Direct Quadrature of the normalised signal is being used to directly yield the angular value $\varphi(x)$.

A limitation occurring in this approach arises from sparse measurements, more specifically, for not having a measurement point exactly at the maxima of the waveform contained in the signal. This causes the wave to be distorted during the scaling process of the AM-FM decomposition. It translates into very sharp peaks in the wavenumber plot which can be alleviated by using a 3 to 5 points median filter (Huang, et al. [24]).

2.2.1. An alternative way to derive the phase angle of the analytic signal for local wavenumber estimation

Considering Eq. (5), which defines the local wavenumber $k(x)$ as the derivative of the angular value $\varphi(x)$ in relation to x, once the angular value is calculated through Eq. (14) or (15) its approximate derivative can be determined numerically by dividing the difference between adjacent points by the spatial step Δx (see Eq. (4)). This is a straightforward implementation with the downside of reducing the spectrum domain by one point. If N points define the sampled signal $F(x)$, the local wavenumbers can only be calculated for $(N-1)$ positions. That is, one wavenumber estimation is performed between every two points of available data.

Alternatively, if an analytical expression is known for the angular value $\varphi(x)$, its derivative can also be determined analytically. In this case, consider Eqs. (5) and (15) with $f_1(x)$ as the analytical expression of $F(x)$ can be rewritten as

$$k(x) = -\frac{f_1^{'}(x)}{\sqrt{1-f_1(x)^2}} \tag{16}$$

Hence, the local wavenumber can be calculated for all sampling points N through Eq. (16) if the derivative $f_1^{'}(x)$ can be determined exactly.

A problem may arise for this expression when x approaches a trough or peak location, x_p. As these are minima and maxima of $f_1(x)$, its derivative $f_1^{'}(x)$ tends to zero and because it is normalised, $f_1(x)^2$ tends to unity, causing both the numerator and the denominator to be zero. L'Hôpital's rule can be applied, leading to

$$k(x_p) = \lim_{x \to x_p} -\frac{f_1^{''}(x)\sqrt{1-f_1(x)^2}}{f_1(x)f_1^{'}(x)} \tag{17}$$

This procedure for calculating the local wavenumber based on the analytical derivative of the angular value is used in the work. The next section clarifies the algorithm used to implement the Direct Quadrature method with this and additional modifications.

2.2.2. Algorithm for the modified direct quadrature method

In this section, additional modifications are proposed to the Direct Quadrature method to make it more suitable to the application at hand. The initial proposed step is to fit a cubic spline function with the purpose of resampling the data points in the signal. In MATLAB, this is achieved by means of the function `csapi` which returns the coefficients of the polynomial function that represents the fitted cubic spline to the input data [28]. Once the spline function is defined, the points of minima and maxima, where the derivative of the function equals zero, are sought and introduced as additional sampling points, increasing the number of data points. This ensures that data points exist at these maxima and minima of the signal and the sparsity measurement problem introduced at the end of the previous section is reduced.

The signal with additional sampling points is truncated to eliminate data points that lie beyond the range defined by the maxima closest to the edges of the absolute value of the signal. This is done because no proper envelope can be defined at those points for the subsequent AM-FM decompositions. Therefore, any approximation of the true envelope would cause distortions to the data at those points during the normalisation step. Fig. 4 shows an example of this distortion. For that reason, a truncation is proposed for the signal to ensure that the initial and end points of the data array contain a peak or valley of the oscillatory function.

The algorithm then performs the AM-FM decomposition of the signal. In this step, unlike originally described for the Direct Quadrature method, the envelope $e(x)$ is only calculated once. The signal $w_2(x)$ resulting from the division between the reference signal and the envelope is evaluated. If $w_2(x)$ is normalised – that is, all values lie within the $[-1;1]$ range – then it is considered as the FM signal. Otherwise, if it is not fully normalised in one iteration, this signal is not considered for the local wavenumber calculation, i.e., it is eliminated from the data set.

The reason for eliminating this signal for the data set and not allowing for an additional normalisation step to occur is that a distortion is created in the signal when the normalisation does not take place in one iteration. This distortion causes a significant deviation in the estimated local wavenumber, which might prevent the localisation of a structural change in the waveguide. This distortion happens because when the normalisation is not fully achieved in one iteration step; it signifies that the envelope is not equal or greater than the magnitude of the signal at a given point, as illustrated in Fig. 5a. This point, at an additional iteration step (shown in Fig. 5b), is considered a point of maximum/minimum value and gets scaled to the value of 1 or -1 even though it was not originally a point of maximum/minimum. Once normalised through additional iteration steps, there occurs an inversion between the original point of maximum and the one point which was normalised in subsequent steps. This is illustrated in Fig. 5c. This inversion between the peak/valley and the adjacent points has a significant effect on the derivative of the angular value $\varphi(x)$, i.e. the local wavenumber, $k(x)$, and thus justifies this data being eliminated from the data set.

For the applications considered in this work, this approach is deemed suitable, as a wide frequency range is considered, and one signal is extracted per frequency, resulting in many available signals. Therefore, as will be seen in the examples within the following sections, eliminating some of those frequencies (and their data) is not problematic for the purpose of locating a structural change in a waveguide through the local wavenumber. That is, the goal can still be achieved with less frequency points being analysed.

After performing the AM-FM decomposition, the normalised signal has the added sampling points removed. This is done to return the sampling array to its original values. This removal is achieved in the same manner as the addition of these points, i.e., a cubic spline function is fitted to the data and the points of maxima/minima are found through the derivative of that function. If they do not correspond to an original measured point, then they are eliminated. In this step, as the normalised signal exists as a fitted cubic spline function, there is an analytical expression to describe it, i.e. the function $f_1(x)$. Therefore, its derivatives used in Eqs. (16) – (17) to determine the local wavenumber can be calculated at this step. The derivatives f_1' and f_1'' are calculated through the MATLAB function `fnder`. In this way, the local wavenumber $k(x)$ can be calculated through Eq. (16) and (17).

Note that, like for the pre-truncated Hilbert transform method, the use of frequency response functions for the modified Direct Quadrature requires its real and imaginary parts to be analysed one at a time and a mean to be performed on the results from both parts. The weighted mean based on the rms values of the original signal at each frequency is proposed in this method as well.

Having detailed the proposed modified Direct Quadrature method, the next section presents numerical examples to evidence how this method performs in estimating the local wavenumber in comparison to the pre-truncated Hilbert transform method.

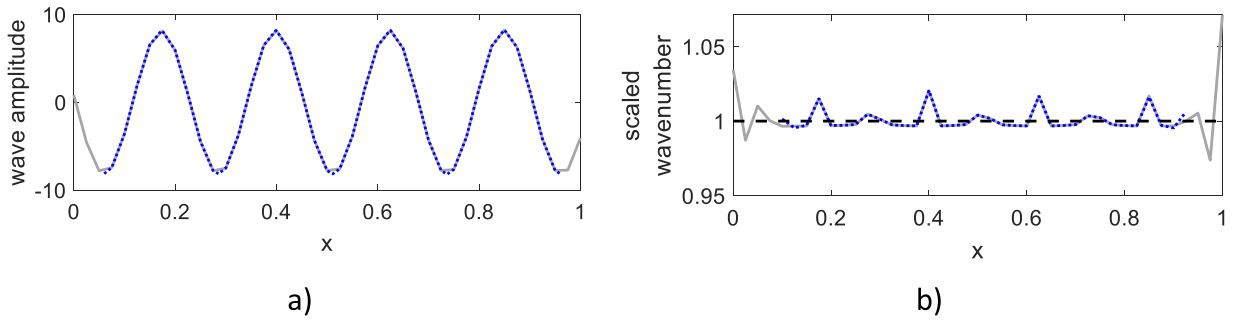

Fig. 4. Effect of truncation in the direct quadrature method: (a) original signal (continuous grey line) and truncated signal (dotted blue line) and (b) resulting scaled wavenumbers with the corresponding lines and reference value (dashed black line).

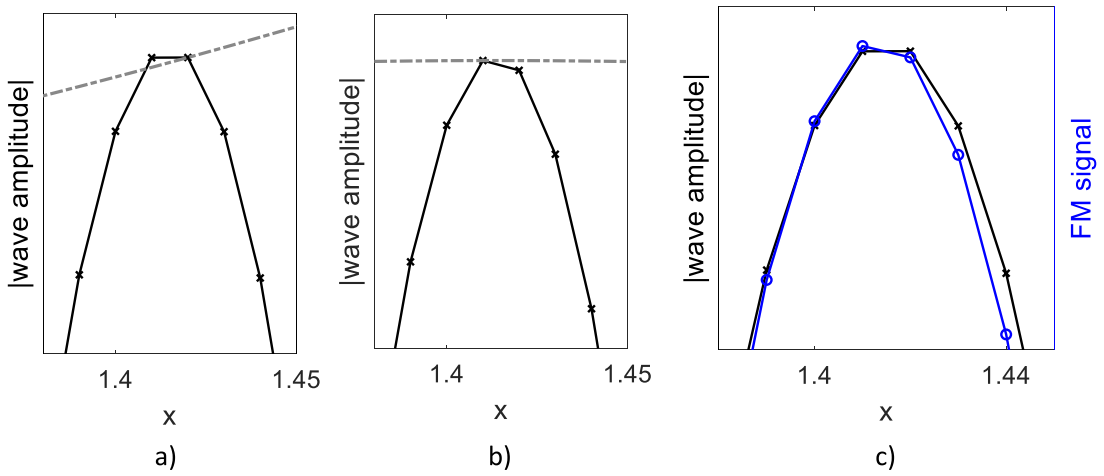

Fig. 5. Inversion of peak location through multiple-step normalisation: (a) sampled original signal (-x- black line) and defined envelope (dash-dot grey line) in step 1, (b) in step 2 where inversion occurs, and (c) comparison of peak position in original (-x- black line) versus normalised function (-o- blue line).

3. Results

The performances of the pre-truncated Hilbert transform method and the modified Direct Quadrature method are evaluated in this section through numerical and experimental analyses. The main objectives are to verify whether these methods can accurately estimate the wavenumbers, in the cases where the wavenumbers are known, and to determine whether discontinuities in the waveguide can be detected through a change caused in the estimated local wavenumbers.

As the results are frequency and spatially dependant, a three-dimensional plot is used throughout the results featuring frequency, distance (between reference and response) and wavenumber. To be able to detect a discontinuity through a change in the local wavenumber where a-priori knowledge of the wavenumber is not available, a graphical aid in the form of a colour scheme is proposed to facilitate the comparison between the estimated wavenumbers.

The colour scheme is used to evidence discrepancies in the estimated wavenumbers along the spatial positions. At each frequency, the mean value of the estimated local wavenumbers is calculated and set as a reference. The differences between the local wavenumbers and the mean wavenumber value are calculated and the point with highest deviation is used to scale the estimated wavenumbers. The result of that scaling ensures that all data points are allocated a value between $[-1;1]$.

Data points with zero-valued wavenumbers are disregarded in this calculation, as they are a result of data that was eliminated at the truncation stages of the two methods. As the main purpose of this colouring scheme is to detect wavenumber deviations that are related to structural changes, a threshold is defined below which all points are attributed the reference colour. This overrules the colours defined in the spectrum and it is done to avoid having small wavenumber deviations that are attributed contrasting colours, i.e., to avoid small errors related to the method or experimental procedure standing out in the plot. Above this threshold the colour spectrum prevails. The magnitude of the threshold is defined on each application, considering the effects of noise, method distortions and change in the local wavenumber due to discontinuity.

3.1. Numerical simulations with the pre-truncated hilbert transform and the modified direct quadrature methods

For the numerical validation, an infinite beam is simulated in two configurations: with and without a discontinuity. These cases are simulated through the analytical expressions that follow. For the infinite beam without any discontinuity [29]:

$$Y_b(x,\omega) = \frac{\omega}{4EIk_b^3}\left[e^{\mp jk_b x} - je^{\mp k_b x}\right] \tag{18}$$

where EI is the flexural stiffness of the beam, k_b is the bending wavenumber of a Euler-Bernoulli beam ($\sqrt[4]{\rho A\omega^2/EI}$) with ρA as the mass per unit length, x is the distance between the output and input and ω is the frequency.

For the infinite beam with a structural change, the discontinuity is introduced through the addition of a point mass at point $x = x_0$, due to its simplicity in modelling and experimental application. The infinite beam with a point mass is modelled through:

$$Y_{x,x_i}(\omega) = Y^b_{x,x_i}(\omega) - \frac{Y^b_{x,x_0}(\omega)Y^b_{x_0,x_i}(\omega)}{Y^m(\omega) + Y^b_{x_0,x_0}(\omega)} \tag{19}$$

where Y is the mobility of the infinite beam with the added mass, Y^b is the mobility of the infinite beam with the response position given by the first subscript and excitation position by the second subscript (calculated through Eq.(18)) and Y^m is the mobility of the

point mass ($1/j\omega m$) with m as the added mass. Positions x_0 and x_i represent the locations of the point mass and the input, respectively. Note that, for cohesiveness, accelerances are obtained from these mobilities and used for the wavenumber extraction seeing that these are the quantities measured in the subsequent experiments.

A steel beam is considered having a rectangular cross section with thickness 6.4 mm, width 5 cm and nominal properties of Young's modulus 210 GPa and density 7900 kgm^{-3}. A spatial length of one metre is considered, with a simulated response at each 25 mm interval, starting at one metre distance from the source location. For the simulation containing a point mass, it is a 22 g mass added arbitrarily at a distance of 1.3 m from the input.

Even though it is not necessary to apply the pre-truncated Hilbert transform method and the modified Direct Quadrature to determine the local wavenumbers in the case of the homogeneous infinite beam without local changes, because the real and imaginary parts of the frequency response function already form an analytic signal, they are used in this work to validate the results against the predictable values. The accelerances obtained from Eq. (18) undergo the processes and methodology described in Section 2, yielding the two dispersion surfaces shown in Fig. 6.

In Fig. 6, a threshold of 5 % for the colouring is used. With the colour scheme in mind, the first observation to be made is that except for a few points at edge positions and at higher frequencies, both methods present results with low deviation (below 5 %) that fit the analytical prediction shown in the black dashed line in Fig. 6b and Fig. 6d.

The lack of estimations at very low frequencies and at edge positions of the surface plot (see plots of Fig. 6a and Fig. 6c) is explained by the limitations of the methods in terms of requiring a full or half wavelength to be contained in the signal for the pre-truncated Hilbert transform and modified Direct Quadrature, respectively. This aspect has been explored in detail in Sections 2.1 and 2.2.

For the simulation of the infinite beam with the point mass, the methods are used with the purpose of locating the position of the added mass through the change caused in the estimated local wavenumbers. Before analysing the wavenumbers resulting from the proposed methods, Fig. 7 shows the plot of the real and imaginary parts of the accelerance at an arbitrary frequency of 1 kHz over the spatial array for the numerical simulation.

From the accelerance plot of Fig. 7, it is possible to note two distinct behaviours, one that occurs between the input and the position

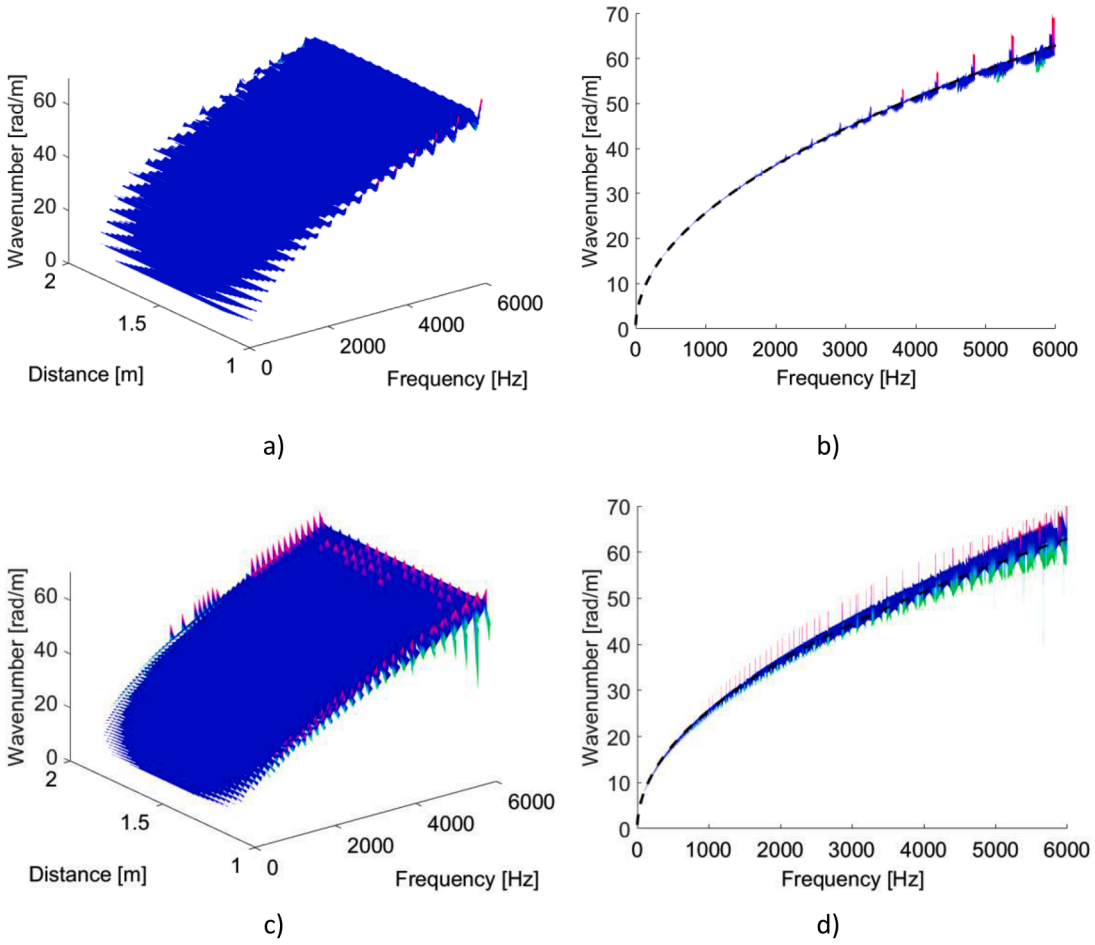

Fig. 6. Numerically obtained local wavenumbers of the infinite beam considering (a) pre-truncated Hilbert transform method and (b) its side view, (c) Direct Quadrature method and (d) side view. Black dashed line in (b) and (d) shows analytic prediction.

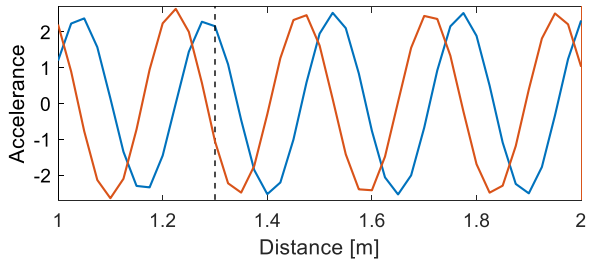

Fig. 7. Real (in blue) and imaginary (in orange) parts of the accelerance of infinite beam with point mass added (position $x_0 = 1.3$ m indicated through dashed line) at an arbitrary frequency.

of the mass [1, 1.3] m and another past the position of the point mass (above 1.3 m). In the first case, the real and imaginary parts of the accelerance no longer form an analytic signal. That is, the imaginary component is not a quadrature of the real component, and thus Eq. (5) cannot be used directly with the accelerances as the analytic signal for the estimation of the local wavenumbers. The visually most significant effect occurs in the amplitudes of those signals and can be interpreted as the effect of superposition of the waves caused by the input and the ones reflected by the point mass. For the points located past the position of the mass (distance greater than 1.3 m) the two signals form an analytic signal, that is, the imaginary component is the quadrature of the real component.

If these accelerances are used directly in Eq. (5) to calculate the local wavenumbers, the results look like what is shown in Fig. 8. This dispersion surface shows that, for the locations between the input and the position of the point mass there are distortions related to wave reflections brought by the added mass that break the quadrature between real and imaginary components of the accelerance. Beyond the position of the point mass, there is a length of the beam over which the results diverge slightly from the expected ones (which could be some near-field effect), but further on the results are as expected.

Alternatively, using the two presented methods to derive the analytic signal based on each part of the accelerance (real and imaginary), one at a time, and averaging the results in accordance to the process described in Section 2 results in the dispersion surfaces is shown in Fig. 9.

From the plots shown in Fig. 9, it can be seen that the position of the point mass coincides with the position where the most significant local wavenumber deviation takes place for both methods. This is shown through the plots (b) and (d) of Fig. 9, as the match between the black line that represents the true location versus the red colouring that indicates the maximum wavenumber deviation.

Comparing the results obtained through the pre-truncated Hilbert transform method and the modified Direct Quadrature method in Fig. 9, it can be seen that the modified Direct Quadrature produces more deviations along the points considered that are not associated with the structural change. This is in accordance with the results shown for the infinite beam in Fig. 6, where the results of the modified Direct Quadrature method present some deviations along the spatial points which stand out at higher frequencies.

3.2. Experiments with the infinite beam

Following the numerical analysis, experiments were performed to verify these methods. The tests were performed with a beam of length 6 m supported by anechoic terminations at its ends to ensure no wave reflections. The beam has the same mechanical properties as that of the numerical simulations in Section 3.1. Considering reciprocity, the accelerances were measured through the roving hammer technique by keeping the accelerometer (type PCB 352A24) at a fixed reference position distanced 0.95 m from the left edge of

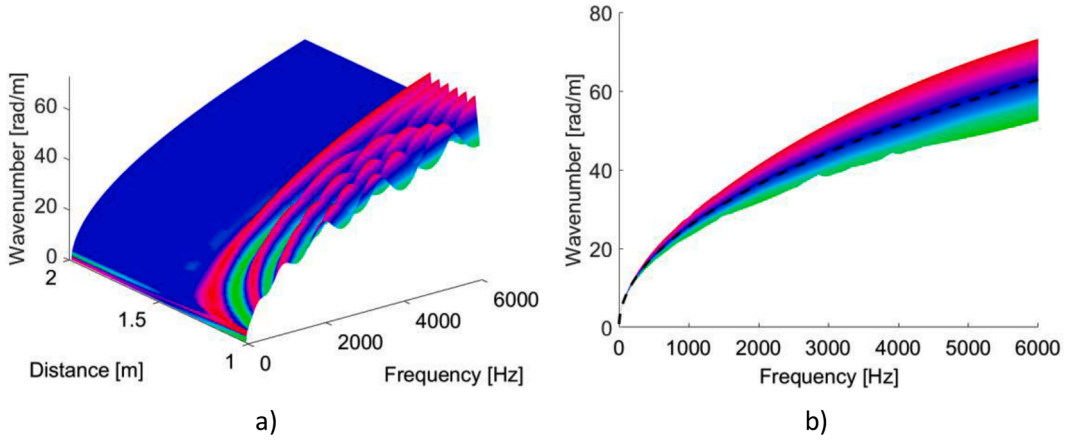

Fig. 8. (a) Numerically obtained local wavenumbers of the infinite beam with point mass (mass location $x_0 = 1.3$ m) considering FRF as analytic signal and (b) side view with black dashed line showing analytic prediction. 1 % colouring threshold.

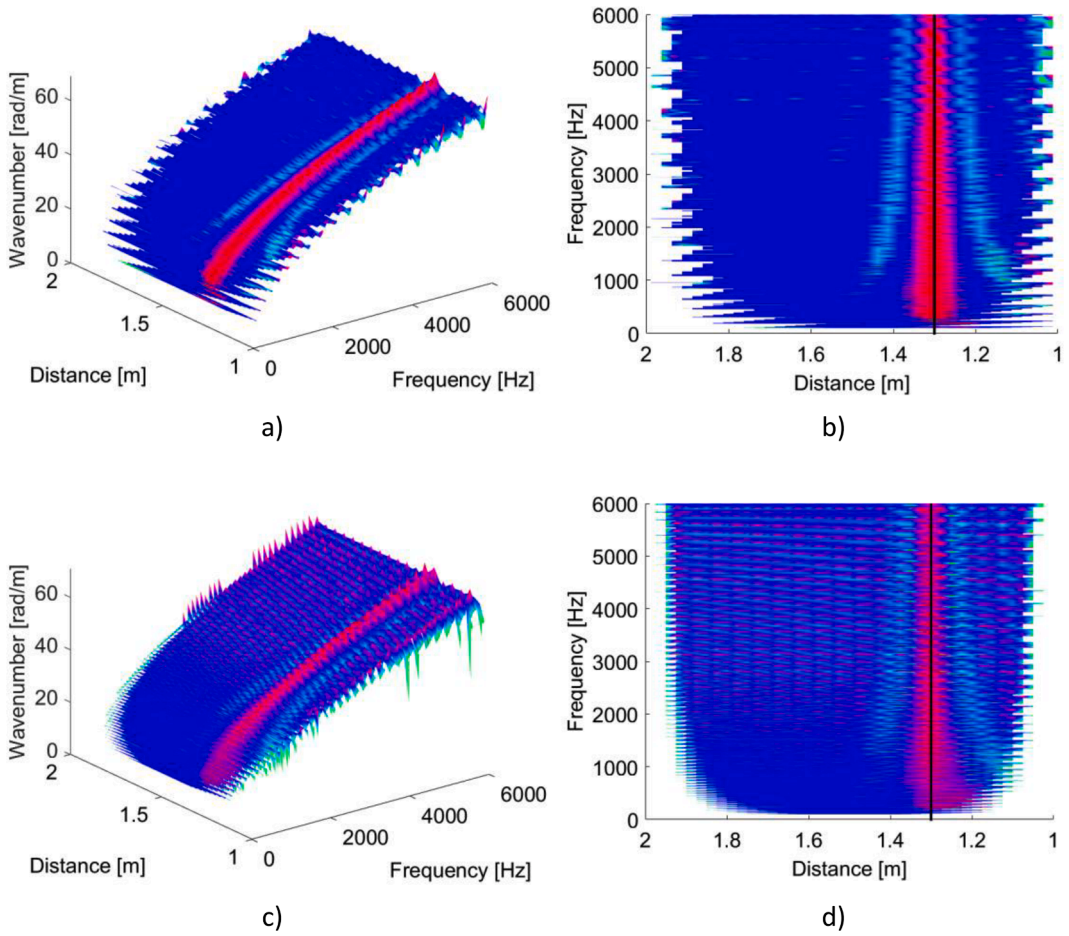

Fig. 9. Numerically obtained local wavenumbers of the infinite beam with point mass ($x_0 = 1.3$ m) through (a) the pre-truncated Hilbert transform method with (b) its top view, (c) the modified Direct Quadrature and (d) its top view. Black continuous line in (b) and (d) shows true position of the mass. 1 % colouring threshold.

the beam. The structure was excited with an instrumented impact hammer PCB 086C01 applied at the measured array length schematically shown in Fig. 10.

Four configurations were investigated, as described in Table 2. The array length contains a total of 41 measurement points, separated at 2.5 cm intervals from one another, measured with a roving hammer technique. It is important to highlight that the roving hammer technique might introduce errors due to mispositioning of the impacts which prevents the intervals from being exactly

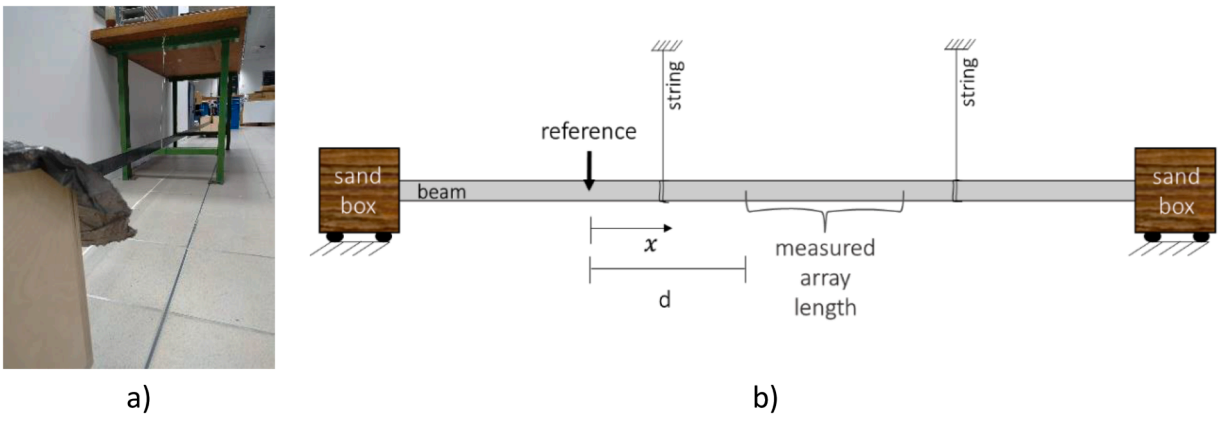

Fig. 10. Picture (a) and illustration (b) of infinite beam test setup with relative position of reference sensor and measured array length.

Table 2
Description of experiments and purpose in the validation of the proposed methods.

Test	Description	Purpose	Distance d [m]	Position of discontinuity [m]
I	No added element	Validate infinite beam results without any added elements	1	–
II	Added 22 g mass	Locate a mass of 22 g within measured array	2.5	2.82
III	Supporting string	Locate the position of the supporting string within measured array	2	2.37

separated by 2.5 cm. Although positioning errors are expected to be negligible compared to the wavelength these may affect the local wavenumber estimation as per Eq. (5). This is mitigated by performing multiple measurements at the same point and averaging them for the determination of the frequency response functions.

The distance between the measured array length and the reference accelerometer varied according to the configuration under test as described in Table 2. Note that a distance is always considered between input and responses and between the measured array and the sand boxes to avoid near-field effects and unwanted reflections, which were seen to distort the local wavenumber estimations in preliminary tests.

3.2.1. Test case i – infinite beam

In the test case I, three methods were used to estimate the local wavenumbers: using the FRF as the analytic signal, applying the pre-truncated Hilbert Transform and applying the modified Direct Quadrature to the FRFs. The latter methods are applied to validate their performance in accurately estimating the local wavenumbers. The results from the three methods are plotted against the analytical predictions in Fig. 11, in which the colouring threshold is set to 10 % for all the plots.

Using the FRF as an analytic signal and extracting the angular phase between every two spatial points (Fig. 11a) is the method that yields the results with highest relative deviation throughout the spectrum. The dominance of the red colouring indicate that the results deviate at relative values that are above 10 % that of the mean at each frequency. The trend, nonetheless, fits the analytic prediction as shown in Fig. 11b. The results at the lowest frequencies were omitted because of large deviations which would hinder the visibility of the plot. This is likely to be due to the effect of reflections of waves that could not be absorbed by the anechoic terminations.

The lack of results observed at the lower and side edges of the dispersion surfaces in plots (c) and (e) of Fig. 11, as explained in Sections 2.1 and 2.2, is related to the truncation necessary to perform these methods.

The results from the pre-truncated Hilbert transform and the modified Direct Quadrature methods, plots (c)-(f) of Fig. 11, are similar to one another and present lower deviations than by using the FRF as an analytic signal. At lower frequencies, the modified Direct Quadrature method presents some points with an amount of deviation higher than 10 %. That indicates that this method could be more sensitive to noise than the pre-truncated Hilbert transform method. At frequencies above 2 kHz both results (Fig. 11d and Fig. 11f) follow the analytical prediction with deviations below the 10 % threshold.

By finding an average maximum deviation for the results with the infinite beam, a new threshold can be defined for each of the methods to ensure that in the following test cases, when a structural change is added to the beam, the colouring scheme highlights only wavenumber deviations that are greater than this baseline deviation. The purpose is to make the local structural change detectable despite possible noise effects. These thresholds are considered by taking an average of the deviations at each location along all frequencies and evaluating the maximum value from all of the location points. For the pre-truncated Hilbert transform method, that value is of 6 %, whereas a percentage value of 10 % is kept for the modified Direct Quadrature method.

Despite the noise and the abovementioned differences between the methods, these experimental results present a good fit to the numerical and analytical ones corroborating this framework as a means to estimate local wavenumbers in an infinite beam.

3.2.2. Test case ii – infinite beam with added local mass

A concentrated mass in the form of a nut of approximately 22 g was attached to the infinite beam for this test case. This mass is equivalent to 0.1 – 8.7 % of the mass of the free uniform beam wavelength to which it is attached in the frequency range up to 6 kHz. This wavelength is determined as the reciprocal of the wavenumbers calculated with the dimensions and material properties described in Section 3.1.

Here a different section of the beam was considered, having the reference sensor distanced by 2.5 metres from the closest measurement point. The nut was attached at a point 2.82 m away from the reference and the FRFs were obtained through a roving hammer test.

Both the pre-truncated Hilbert transform method and the modified Direct Quadrature were applied considering these FRFs yielding the results shown in Fig. 12.

These results show a visible increase in the wavenumbers at the position where the mass was added, evidenced by the match of the red region and black line on plots (c) and (d) of Fig. 12. Thus showing that the mass could be located through both methods.

There are visible deviations in the wavenumbers at a distance around 3 and 3.2 m from the reference, shown in green on the plots, which are not associated with any external structural change. No further investigation was performed to determine whether it is associated with noise or some internal property of the waveguide. Nonetheless, it is possible to conclude that if the structural change that is to be located through this method does not provoke a significant change in the wavenumbers, then it is possible that deviations brought by other factors such as noise or other differences in local properties might be evidenced and make a proper localisation of the structural change more difficult.

Comparing the results of both methods, the main difference lies in the magnitude of the variation of the wavenumbers along the

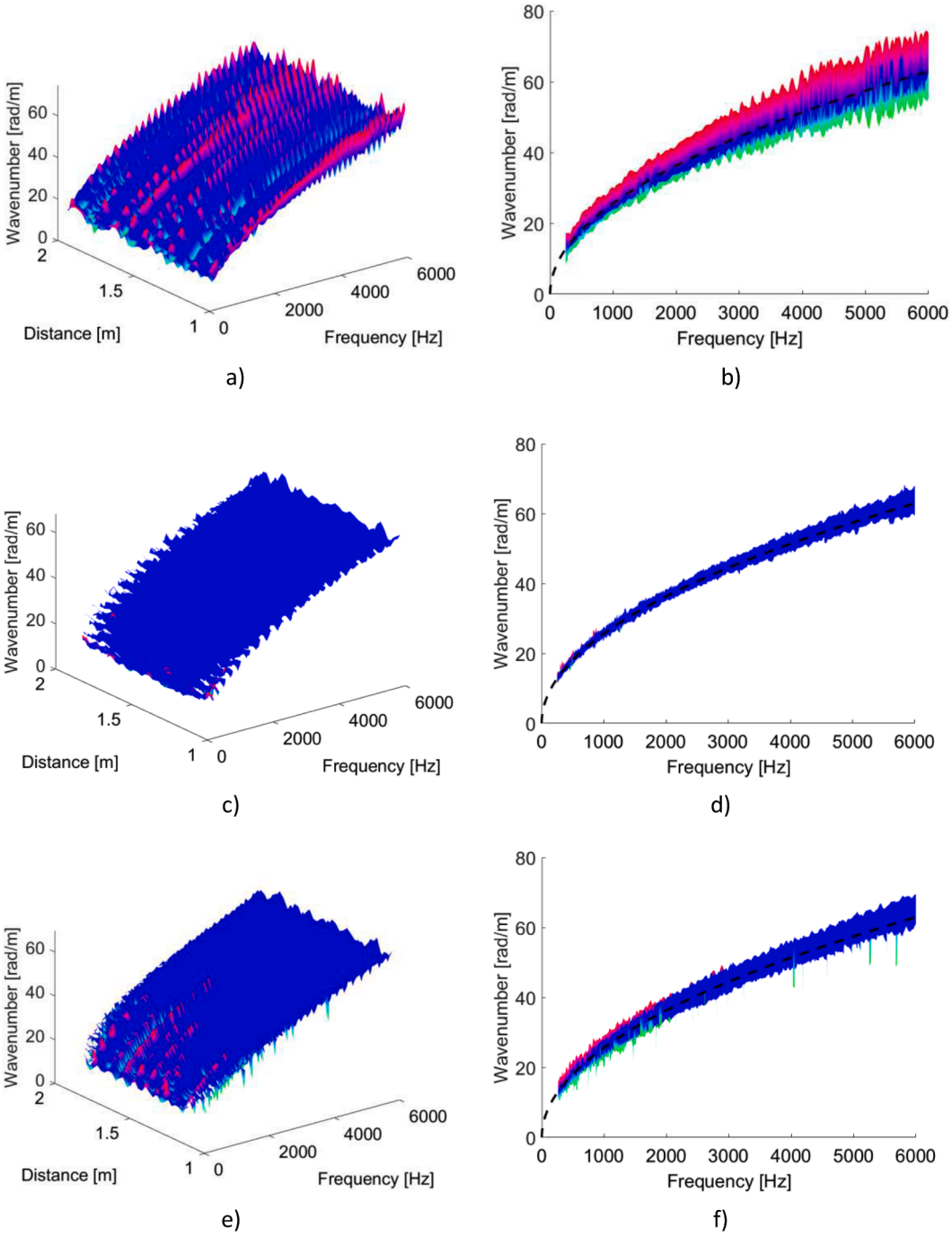

Fig. 11. Experimentally obtained local wavenumbers of the infinite beam considering (a) FRF as analytic signal and (b) its side view, (c) pre-truncated Hilbert transform method and (d) its side view and (e) modified Direct Quadrature method and (f) its side view. Black dashed line on (b), (d) and (f) shows the analytic prediction.

spatial locations. Even setting a higher colour threshold of 10 % for the modified Direct Quadrature, versus 6 % for the pre-truncated Hilbert Transform, the deviations at position around 3.2 m are dominant up to 2 kHz though that method.

3.2.3. Test case iii – infinite beam and the supporting string

In test case III, the string used to support the beam was considered as an alternative type of discontinuity in the waveguide. Once again, the proposed methods are applied with the means of locating the string that is used to support the beam. The pre-truncated Hilbert transform method and the modified Direct Quadrature method applied to the obtained FRFs resulting in the surfaces shown

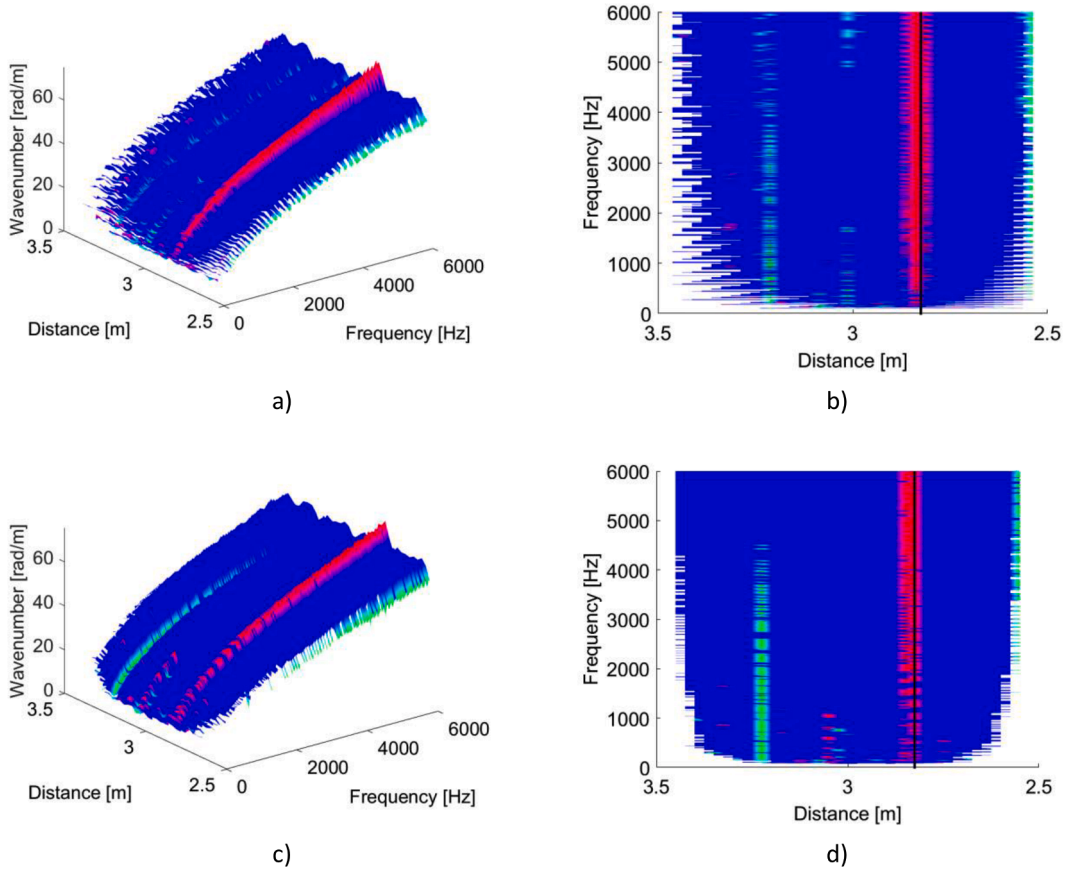

Fig. 12. Local wavenumber results from (a) pre-truncated Hilbert transform and (b) its top view, (c) modified Direct Quadrature method and (d) its top view. Position of nut ($x_0 = 2.82$ m) indicated through (continuous black line) in (b) and (d). Colour thresholds of 6 % for pre-truncated Hilbert transform and 10 % for modified Direct Quadrature.

in Fig. 13.

The effect of the supporting string on the local wavenumbers is discernible in the results shown in Fig. 13. As it happens for the added point mass, there is an increase in the estimated local wavenumber associated with the supporting string and in this case, no spurious positions are evidenced in the plot.

There is a slight offset between the position of the maximal wavenumber deviation and the true position of the string of approximately 1 cm, which would yield a 0.4 % error in the localisation, at medium to higher frequencies for the pre-truncated Hilbert transform method and throughout the frequency spectrum of the Direct Quadrature method results. Due to the low magnitude of the error, this was not further investigated in this work.

Through these experiments, the proposed methods were shown to be able to estimate the local wavenumbers of the infinite waveguide and to locate the position of a local structural change in the form of an added mass and supporting string, when proper consideration is given to the input position and to the amount of noise versus structural change effect on the local wavenumbers.

4. Conclusions

In this work, the problem of locating a discontinuity in a waveguide based on estimation of the experimental local wavenumber was considered. This problem can be divided into (i) accurately estimating local wavenumbers and (ii) investigating divergences in the wavenumbers brought about by local structural changes. For wavenumber estimation (i), modifications to the Hilbert transform frequency-domain estimator and to the Direct Quadrature method were proposed, while divergence (ii) was investigated through numerical and experimental analysis. The results have shown that the proposed modifications enable an accurate estimation of the local wavenumbers of an infinite-like one-dimensional structure. Likewise, a discontinuity in the form of a local mass or support could be located by tracking wavenumber changes along the structure. It was also observed that spurious distortions can exist brought about by noise and near-field effects of the input and they should be avoided for a proper localisation of the structural change by ensuring their effect is smaller than the one of the structural change or is placed outside the measuring length.

These developments hold importance in various fields, where the methods can be applied to improve remote monitoring to optimise performance and maintenance of structural components. Further understanding of the types and magnitudes of

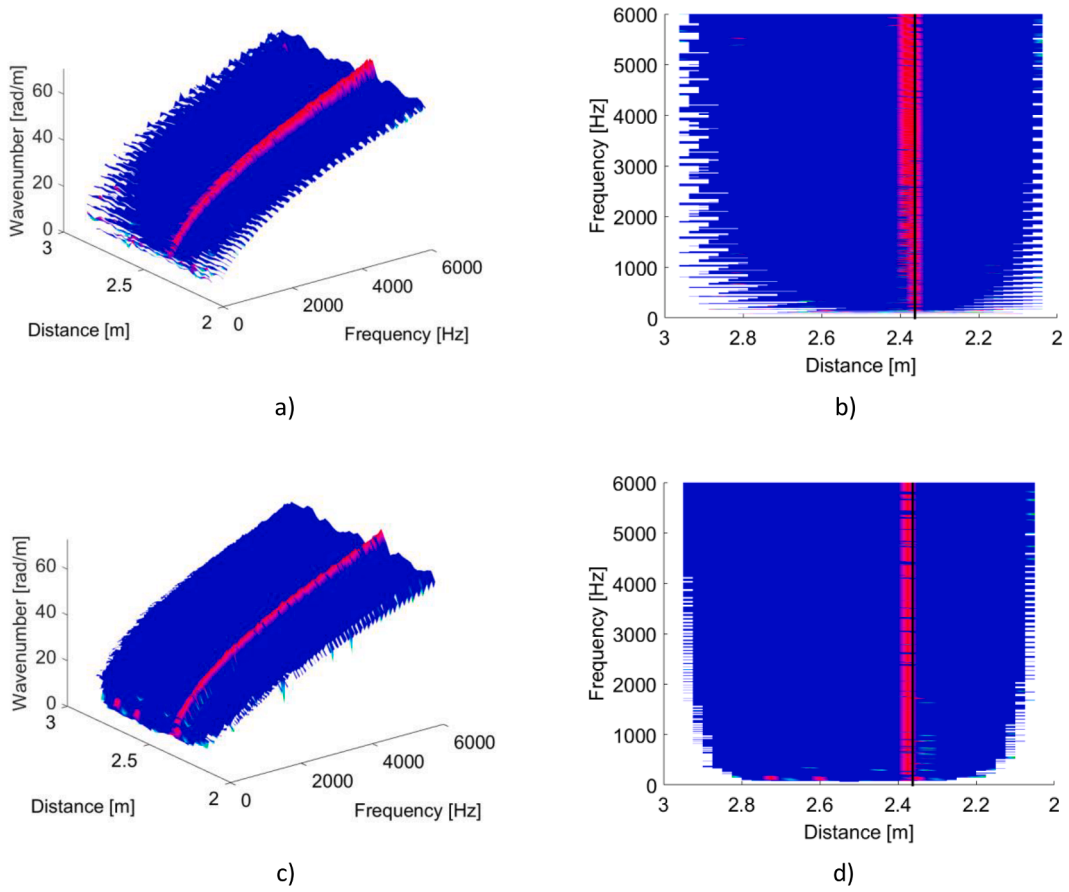

Fig. 13. Local wavenumber results from (a) pre-truncated Hilbert transform and (b) its top view, (c) modified direct quadrature method and (d) its top view. Position of string ($x_0 = 2.37$ m) indicated through (-) in (b) and (d). Colour thresholds of 6 % for pre-truncated Hilbert transform and 10 % for modified Direct Quadrature.

discontinuities that can be located through these methods, considering the effect of noise, and applicability to finite structure are topics to be investigated in future research.

CRediT authorship contribution statement

M.W. Bavaresco: Conceptualization, Investigation, Methodology, Software, Validation, Writing – original draft. **E. Rustighi:** Conceptualization, Methodology, Resources, Supervision, Writing – review & editing. **N.S. Ferguson:** Conceptualization, Methodology, Project administration, Resources, Supervision, Writing – review & editing.

Declaration of competing interest

The authors declare that they have no known competing financial interests or personal relationships that could have appeared to influence the work reported in this paper.

Data availability

Data will be made available on request.

Acknowledgements

This paper is supported by the European Union's Horizon 2020 research and innovation programme under the Marie Skłodowska-Curie grant agreement No 765636, project InDEStruct (Integrated Design of Engineering Structures).

References

[1] H. Li, X. Xiao, D. Thompson, G. Squicciarini, The sound radiation from a periodic array of railway sleepers using a wavenumber domain method, J. Sound Vib. 561 (2023) 117818, https://doi.org/10.1016/j.jsv.2023.117818.

[2] J. Spytek, L. Ambrozinski, L. Pieczonka, Evaluation of disbonds in adhesively bonded multilayer plates through local wavenumber estimation, J. Sound Vib. 520 (2022) 116624, https://doi.org/10.1016/j.jsv.2021.116624.

[3] M.K. Kalkowski, J.M. Muggleton, E. Rustighi, An experimental approach for the determination of axial and flexural wavenumbers in circular exponentially tapered bars, J. Sound Vib. 390 (2017) 67–85, https://doi.org/10.1016/j.jsv.2016.10.018.

[4] O. Mesnil, C.A. Leckey, M. Ruzzene, Instantaneous and local wavenumber estimations for damage quantification in composites, Structural Health Monitoring 14 (3) (2015) 193–204, https://doi.org/10.1177/1475921714560073.

[5] J. Berthaut, M. Ichchou, L. Jézéquel, Wavenumbers identification in two-dimensional structures: comparison between two new methods, in: Proceedings of the Tenth International Congress on Sound and Vibration, Stockholm, Sweden, 2003, pp. 1155–1162.

[6] R. Boukadia, F.C. Claeys, C. Droz, M. Ichchou, W. Desmet, E. Deckers, An inverse COnvolution MEthod for wavenumber extraction (INCOME): formulations and applications, J. Sound Vib. (2021) 116586, https://doi.org/10.1016/j.jsv.2021.116586.

[7] N.S. Ferguson, C.R. Halkyard, B.R. Mace, K.H. Heron, The estimation of wavenumbers in two-dimensional structures, in: Proceedings of Isma2002: International Conference on Noise and Vibration Engineering, Leuven, Belgium 1-5, 2002, pp. 799–806. Vols.

[8] X. Li, M. Ichchou, A. Zine, N. Bouhaddi, P. Fossat, Wavenumber identification of 1D complex structures using Algebraic Wavenumber Identification (AWI) technique under complex conditions, J. Sound Vib. 548 (2023) 117524, https://doi.org/10.1016/j.jsv.2022.117524.

[9] J.M. Muggleton, M.J. Brennan, P.W. Linford, Axisymmetric wave propagation in fluid-filled pipes: wavenumber measurements in in vacuo and buried pipes, J. Sound Vib. 270 (1–2) (2004) 171–190, https://doi.org/10.1016/S0022-460X(03)00489-9.

[10] G. Zhao, B. Wang, W. Hao, Y. Luo, H. Chen, Localization and characterization of delamination in laminates using the local wavenumber method, Compos. Struct. 238 (2020), https://doi.org/10.1016/j.compstruct.2020.111972.

[11] M.D. Rogge, C.A.C. Leckey, Characterization of impact damage in composite laminates using guided wavefield imaging and local wavenumber domain analysis, Ultrasonics 53 (7) (2013) 1217–1226, https://doi.org/10.1016/j.ultras.2012.12.015.

[12] E.B. Flynn, S.Y. Chong, G.J. Jarmer, J.-R. Lee, Structural imaging through local wavenumber estimation of guided waves, NDT & E International 59 (2013) 1–10, https://doi.org/10.1016/j.ndteint.2013.04.003.

[13] T. Gao, H. Sun, Y. Hong, X. Qing, Hidden corrosion detection using laser ultrasonic guided waves with multi-frequency local wavenumber estimation, Ultrasonics 108 (2020) 106182, https://doi.org/10.1016/j.ultras.2020.106182.

[14] Z. Tian, W. Xiao, Z. Ma, L. Yu, Dispersion curve regression – assisted wideband local wavenumber analysis for characterizing three-dimensional (3D) profile of hidden corrosion damage, Mech. Syst. Signal Process. 150 (2021) 107347, https://doi.org/10.1016/j.ymssp.2020.107347.

[15] J. He, X. Liu, Q. Cheng, S. Yang, M. Li, Quantitative detection of surface defect using laser-generated Rayleigh wave with broadband local wavenumber estimation, Ultrasonics 132 (2023) 106983, https://doi.org/10.1016/j.ultras.2023.106983.

[16] M. Feldman, Hilbert Transform Applications in Mechanical Vibration, Wiley, Hoboken, N.J., 2011.

[17] N.E. Huang, et al., The empirical mode decomposition and the Hilbert spectrum for nonlinear and non-stationary time series analysis, in: Proceedings of the Royal Society of London. Series A: Mathematical, Physical and Engineering Sciences 454, 1998, pp. 903–995, https://doi.org/10.1098/rspa.1998.0193.

[18] N.E. Huang, S.S.P. Shen, Hilbert-huang Transform And Its Applications, World Scientific Publishing Company, Singapore, SINGAPORE, 2005.

[19] N.E. Huang, Z. Shen, S.R. Long, A NEW VIEW OF NONLINEAR WATER WAVES: the Hilbert Spectrum, Annu. Rev. Fluid Mech. 31 (1) (1999) 417–457, https://doi.org/10.1146/annurev.fluid.31.1.417.

[20] S.T. Quek, P.S. Tua, Q. Wang, Detecting anomalies in beams and plate based on the Hilbert–Huang transform of real signals, Smart Mater. Struct. 12 (3) (2003) 447–460, https://doi.org/10.1088/0964-1726/12/3/316.

[21] S. Bandara, P. Rajeev, E. Gad, B. Sriskantharajah, I. Flatley, Damage detection of in service timber poles using Hilbert-Huang transform, NDT & E International 107 (2019) 102141, https://doi.org/10.1016/j.ndteint.2019.102141.

[22] Y. Lugovtsova, J. Bulling, O. Mesnil, J. Prager, D. Gohlke, C. Boller, Damage quantification in an aluminium-CFRP composite structure using guided wave wavenumber mapping: comparison of instantaneous and local wavenumber analyses, NDT & E International 122 (2021) 102472, https://doi.org/10.1016/j.ndteint.2021.102472.

[23] C.C. Craciunescu, M. Christou, On the calculation of wavenumber from measured time traces, Appl. Ocean Res. 98 (2020) 102115, https://doi.org/10.1016/j.apor.2020.102115.

[24] N.E. Huang, Z. Wu, S.R. Long, K.C. Arnold, X. Chen, K. Blank, On instantaneous frequency, Adv. Adapt. Data Anal. 01 (02) (2009) 177–229, https://doi.org/10.1142/S1793536909000096.

[25] D. Gabor, Theory of communication, Journal of the Institution of Electrical Engineers - Part I: General 94 (1946) 58, https://doi.org/10.1049/ji-1.1947.0015.

[26] J.S. Bendat, A.G. Piersol, Random Data: Analysis and Measurement Procedures, John Wiley & Sons, Inc., New York, 2000.

[27] P. Cheh, Gibbs phenomenon removal and digital filtering directly through the fast Fourier transform, IEEE Trans. Signal Process. 49 (2) (2001) 444–448, https://doi.org/10.1109/78.902128.

[28] T. M. Inc., *Curve Fitting Toolbox 2021a*. Available: https://uk.mathworks.com/help/curvefit/index.html (July 2023).

[29] F. Fahy, P. Gardonio, Sound and Structural Vibration, 2nd Edition, Academic Press, London, UK, 2006.